

Recovering waste energy of the combined gas turbine system using paraffin melting

Y. S. Najjar¹ and A. S. Irbai^{2*}

¹ Mechanical Engineering Department, Jordan University of Science and Technology, Irbid, Jordan

² Mechanical Engineering Department, School of Engineering Technology, Al Hussein Technical University, Amman, Jordan

ABSTRACT – This work covers waste energy utilization of the combined power cycle by using it in the candle raw material (paraffin) melting process and an economic study for this process. After a partial utilization of the burned fuel energy in a real bottoming steam power generation, the exhaust gas contains 0.033 of the initially burned energy. This tail energy with about 128 °C is partly driven in the heat exchanger of the paraffin melting system. Ansys-Fluent Software was used to study the paraffin wax melting process by using a layered system that utilizes an increased interface area between the heat transfer fluid (HTF) and the phase change material (PCM) to improve the paraffin melting process. The results indicate that using 47.35 kg/s, which is 5% of the entire exhaust gas (881.33 kg/s) from the exit of the combined power cycle, would be enough for producing 1100 tons per month, which corresponds to the production quantity by real candle's factories. Also, 63% of the LPG cost will be saved, and the payback period of the melting system is 2.4 years. Moreover, as the exhaust gas temperature increases, the consumed power and the payback period will decrease.

ARTICLE HISTORY

Received: 13th Feb 2020

Revised: 27th June 2020

Accepted: 04th July 2020

KEYWORDS

*Combined power cycle;
heat recovery;
paraffin melting*

INTRODUCTION

Renewable energy cannot be used for the intensive use of power generation with sustainable thermo-economic results. Therefore, energy efficiency is considered the most suitable in the transition period toward a higher portion era. Three ways are used to enhance the energy efficiency of the gas turbine power plant: waste heat recovery, using thermal energy storage, and cooling compressor inlet air, which reduces the compression power.

Najjar et al. [1]–[6] enhanced the gas turbine power plant by recovering waste energy to cool compressor inlet air. Najjar and Abubaker [1] used an indirect evaporative cooling system to cool the compressor inlet temperature. They compared a combination of the indirect evaporative cooling system (IECS) and absorption chiller with a combination of IECS and mechanical chiller.

Najjar and Zaamout [2] enhanced the gas-turbine by using water injection in a regenerative cycle and utilizing the exhaust waste energy in the recuperator and the water-heater. They found that the compressor pressure-ratio outperforms the compressor pressure-ratio by about 57% in power and 13% in efficiency, and that water injection would compensate for the power de-rating of engines during the hot season.

Najjar and Abubaker [3] analyzed the exergy of a cascade - waste heat recovery system for compressor inlet air cooling and power generation. The cascade system consists of an organic Rankine cycle and refrigeration cycle. The working fluid in both cycles is propane. They found that the power plant efficiency can be increased by up to 50%.

Singh [7] utilized the exhaust gas from the combined cycle to operate aqua ammonia absorption chiller in addition to compressor inlet air cooling to improve the Brayton-Rankine combined cycle power plants. He did the energy and exergy analysis during the summer and winter. He found that thermal efficiency increased by about 1.2% in the summer.

Several researchers utilize the exhaust gas with low temperature to produce power, cooling loads, heating loads, or a combination of them. Carcasci and Winchler [8] recovered low-temperature waste energy from intercooler gas turbines using the Organic Rankine Cycle combined with four different organic fluids. They found that this process will increase the global power plant efficiency. Bălănescu and Homutescu [9] analyzed adding both Steam Rankine Cycle and Organic Rankine Cycle as a bottoming cycle for gas turbine (Brayton) cycle for recovering waste heat. They found that the efficiency of the power plant increases by 1 %.

Ipakchi et al. [10] utilized waste heat for combined cooling and power by using transcritical CO₂ ejector. They found that the net present value and the simple payback period of the proposed system are equal to 0.3419 M\$ and about four years and six months, respectively. Han et al. [11] studied a novel combined power and long-distance heating/cooling system without heat preservation. Their proposed system integrates the Kalina cycle with the solution energy storage cycle. They found that the thermal insulation is unnecessary, and the pipe diameter is reduced.

Huang et al. [12] analyzed the gas turbine combined cycle based on the utilization of waste energy for combined cooling, heating, and power. They used the turbine inlet temperature (TIT) strategy and inlet guide vanes (IGV) strategy for the gas turbine to adopt the part-load performance. They found that IGV plays a role in increasing the steam turbine

power output and reducing the exhaust heat in HRSG, but causes more exergy destruction in the steam turbine expansion process, and the IGV strategy reinforces the part-load performance of the CCHP system.

Hou et al. [13] analyzed a combined cooling, heating and power system driven by gas turbine waste heat is discussed. They found that the optimum values of total product unit cost and total heat exchanger area per unit exergy output are 10.0526 \$/GJ and 0.1755m²/kW, respectively. The result also indicates that by using the CCHP system, 4.9901MW of power, 0.584MW of heat capacity, and 0.627MW of refrigeration capacity can be recovered from the exhaust gas. Dehghan [14] recovered the waste exhaust heat from a micro gas turbine by using a ground source heated pump system. This system is used to store the wasted heat in the ground during hot days and extract it during cold days. He found that this system is recommended for building and has a low back period.

Thermal energy storage systems can also be used to improve the performance of power plants. These systems divide into pressured, heated and heated pressured thermal energy storage systems. Yang et al. [15] studied a combination of a solar collector and a compressed air energy storage system added to the gas turbine power plant. Wang et al. [16] analyzed a combination of a solar compressed energy storage system with an organic Rankine cycle and gas turbine plant. They found that increasing the compression ratio raises the energy efficiency of this combination. Whereas, increasing turbines inlet temperature decrease it.

Grange et al. [17] analyzed a hybrid system that consists of a solar power plant and packed bed thermal energy storage. This hybrid system is used to offer a stable and higher electrical power source. Abarr et al. [18] recovered and used the waste heat of the gas turbine with pumped thermal energy storage that consists of a compressor, expander, cold thermal energy storage, and hot thermal energy storage. The working fluid (ammonia) extracts the heat from the turbine exhaust temperature and stores it in concrete. They used Solid Work finite element analysis to study the thermal energy storage.

In this work, the waste heat of the combined power cycle is recovered to utilize in an industrial process. A candle melting system is added to the combined power cycle that has constant exhaust temperature. Ansys-Fluent Software is used to study the paraffin wax melting process that similar to the thermal energy storage systems. A system that utilizes metallic fins and increasing the interface area between the heat transfer fluid (HTF) and the phase change material (PCM) is used to improve the paraffin melting process. Also, a compressor with a variable guide vane is utilized with the gas turbine and controlled to produce constant exhaust temperature.

THEORETICAL ANALYSIS

Process Sequence

In this work, a paraffin melting system is used with a combined power cycle to utilize exhaust energy, as shown in Figure 1. A variable guide vane compressor is used with the gas turbine and controlled to produce constant exhaust temperature. This energy is partially utilized in the bottoming cycle of steam power generation. The tail energy with about 128 °C is partly derived in the paraffin melting in the candle's factory.

As shown in Figure 2, the variable guide vanes use the air mass flow rate of the compressor to control the generated power and produce exhaust gas at a constant temperature. For reducing the power generation at part load, it enters a smaller air flow rate to the compressor. The exhaust gas temperature (EGT) is constant when the generated power between 30%-90% of the full load. The minimum flow rate is 60% of the maximum value, and it happens when the generated power is 30% ,[19]. This way enhances flow and speed upgrades and increases the generated power at full load. Using energy storage systems with this technology is not useful because the exhaust gas always is available, and it has a constant temperature. The entered air to the compressor (state 1) is compressed to state 2. The compressed air is mixed with the fuel and burned in the combustor. The combustion gases (state 3) enters the gas turbine and leaves the turbine at state 4.

The exhaust gases respectively enter the high pressure, low-pressure steam generator and preheater to recover the heat and generate water steam and exit at state 5. Part of this exhaust gas enters a compact heat exchanger at state 6 and leaves it to the atmosphere at state 8 for heating the heat transfer fluid (HTF). This HTF enters the heat exchanger at state 9 and exits at state 10 for melting the paraffin wax. In the Rankine cycle, condensed water at state 21 is pressured to state 11 using the pump. Pressured water enters the preheater and leaves at state 12. After that, it enters the low-pressure steam generator and leaves at state 13, which is divided into two parts. The first part (state 18) enters the low-pressure steam turbine, whereas the second part (state 14) is pumped to state 15. After that, water at state 15 enters the high-pressure steam generator and leaves it at state 16 as steam. This part that enters the high-pressure steam turbine is partially expanded to state 17. States 18 and 17 are mixed to form state 19, which enters the low-pressure steam turbine and expands to state 20 then enters the condenser. Electric generators convert the gas and steam turbines shafts rotation to power.

Figure 3 shows the paraffin wax melting system. The HTF enters the layered system and heats the PCM. After that, the HTF exists and returns to the heat exchanger. This process continues until melting the paraffin wax.

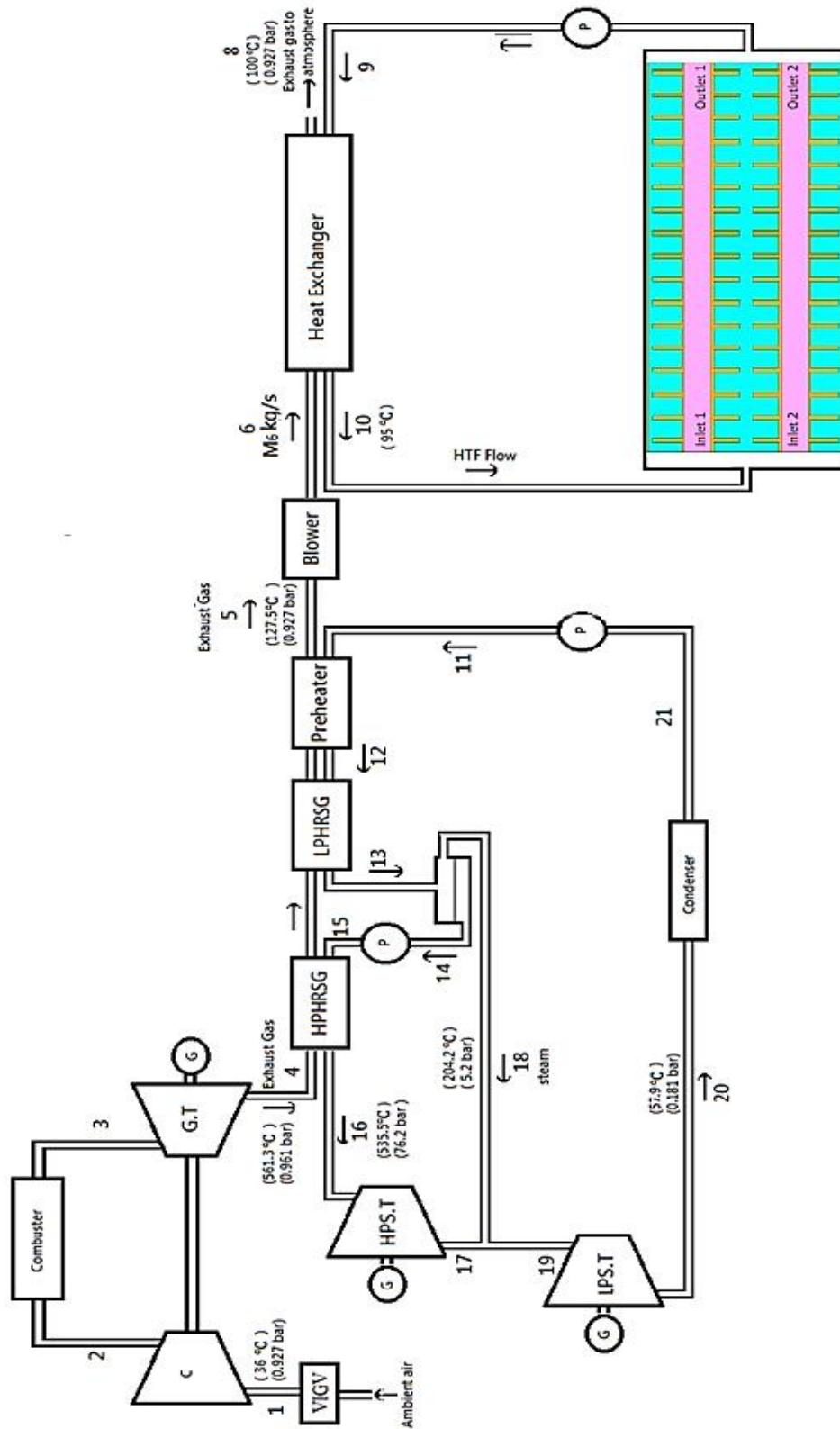


Figure 1. Utilization of exhaust gas thermal energy to generate the cooling/heating load for the combined station buildings

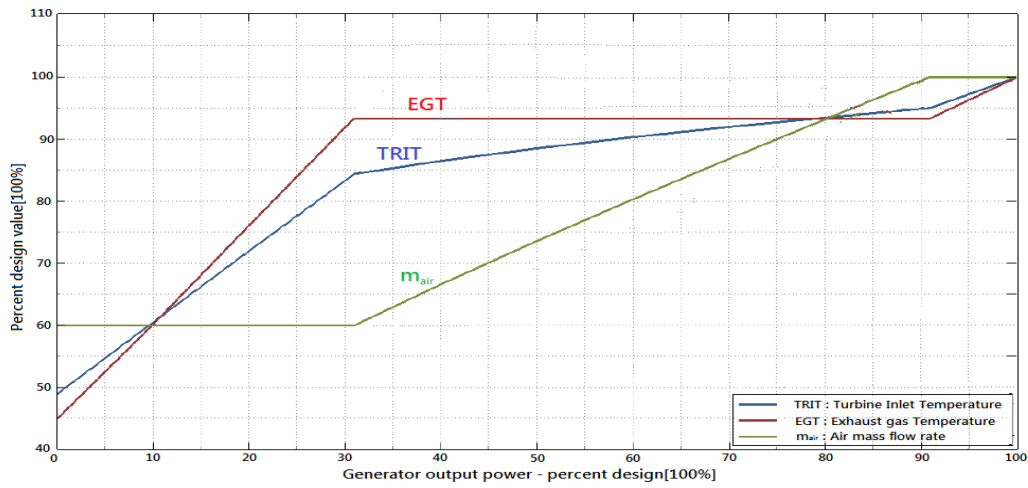


Figure 2. Engine control curves [19]

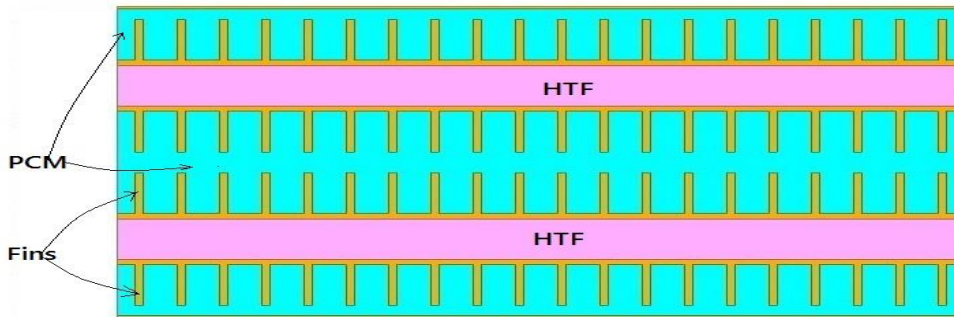


Figure 3. Geometry of paraffin wax melting container

Paraffin Melting System

As shown in Figure 3, the layered container consists of rectangular channels. Hence the green, brown and pink are stationary paraffin wax powder, metallic fins, and HTF, respectively. The container dimensions are 0.2 x 0.5 x 5 (height x width x depth). The top and bottom container walls are assumed adiabatic. Moreover, Table 1 shows the physical properties of HTF, finned ducts, and paraffin wax [20]–[22]. These physical properties are assumed to be constant except the density, which changes based on the Boussinesq model.

Table 1. Physical properties of used materials

Property	Unit	Water	Copper	Stainless Steel	Paraffin wax (Suntech P116)
Density	kg/m ³	998	8300	8030	818 (solid) 760 (liquid)
Specific Heat	J/kg.K	4183	419	502.5	2950
Thermal Conductivity	W/m.K	0.6	372	16.27	0.24
Heat of Fusion	J/kg	-	-	-	266000
Solidification Temperature	K	-	-	-	316
Melting temperature	K	-	-	-	329
Thermal Expansion	1/K	-	-	-	0.002
Dynamic Viscosity	kg/m.s	89 x 10 ³	-	-	1.9

Assumptions

1. Laminar incompressible flow
2. negligible viscous dissipation
3. Boussinesq model for natural convection
4. No edge effects

Melting System Analysis

The compact heat exchanger is used to heat the HTF to 368.15 K. The pumping power and pressure drop through the melting container are calculated by using:

Internal flow pressure drop is equal to [23] :

$$\Delta P_{Internal} = f \frac{\rho V_{mean}^2}{2D} \Delta L \tag{1}$$

External flow pressure drop is equal to [23] :

$$\Delta P_{External} = f N_L x \frac{\rho V_{max}^2}{2} \tag{2}$$

where the friction and correction factors (f, x) are obtained from [23].

The consumed power is equal to:

$$Power = \frac{\text{fluid flow rate}}{\text{device efficiency} \cdot \text{fluid density}} \sum (\Delta P_{internal} + \Delta P_{External}) \tag{3}$$

The pressure drop through the compact heat exchanger is calculated by [23] :

$$\Delta P = f \left(\frac{M}{\sigma A_{fr}} \right)^2 \frac{\alpha V_L (v_i + v_o)}{2 \sigma A_{fr} \cdot 2} \tag{4}$$

The continuity and momentum and energy equations that describe the melting process are [24]:

The continuity equation is:

$$\frac{\partial \rho}{\partial t} + \frac{\partial(\rho V_x)}{\partial x} + \frac{\partial(\rho V_y)}{\partial y} = 0 \tag{5}$$

The momentum equations are :

in x-direction

$$\rho \left(\frac{\partial V_x}{\partial t} + V_x \frac{\partial V_x}{\partial x} + V_y \frac{\partial V_x}{\partial y} \right) = - \frac{\partial p}{\partial x} + \left(\frac{\partial \tau_{xx}}{\partial x} + \frac{\partial \tau_{xy}}{\partial y} \right) + \rho g_x + S_m \tag{6}$$

in y-direction

$$\rho \left(\frac{\partial V_y}{\partial t} + V_x \frac{\partial V_y}{\partial x} + V_y \frac{\partial V_y}{\partial y} \right) = - \frac{\partial p}{\partial y} + \left(\frac{\partial \tau_{xy}}{\partial x} + \frac{\partial \tau_{yy}}{\partial y} \right) + \rho g_y + S_m \tag{7}$$

For the Newtonian fluid having constant density and viscosity, Eqs. (6) and (7) become:

in x-direction

$$\rho \left(\frac{\partial V_x}{\partial t} + V_x \frac{\partial V_x}{\partial x} + V_y \frac{\partial V_x}{\partial y} \right) = - \frac{\partial p}{\partial x} + \mu \left(\frac{\partial^2 V_x}{\partial x^2} + \frac{\partial^2 V_x}{\partial y^2} \right) + \rho g_x + S_m \tag{8}$$

in y-direction

$$\rho \left(\frac{\partial V_y}{\partial t} + V_x \frac{\partial V_y}{\partial x} + V_y \frac{\partial V_y}{\partial y} \right) = - \frac{\partial p}{\partial y} + \mu \left(\frac{\partial^2 V_y}{\partial x^2} + \frac{\partial^2 V_y}{\partial y^2} \right) + \rho g_y + S_m \tag{9}$$

where $S_m = c_{mushy} \frac{(1-Y)^2}{0.001+Y^3} \vec{V}$

Where, c_{mushy} is the constant of transition that reduces the velocity to zero as PCM solidifies, and Y is the volume fraction of liquid.

$$\text{where } Y = \begin{cases} \frac{T-T_s}{T_m-T_s}, & T_s < T < T_m \\ 0 & , T < T_s \\ 1 & , T > T_m \end{cases}$$

The energy equation is :

$$\begin{aligned} \rho C_p \left(\frac{\partial T}{\partial t} + V_x \frac{\partial T}{\partial x} + V_y \frac{\partial T}{\partial y} \right) &= - \left(\frac{\partial q_x}{\partial x} + \frac{\partial q_y}{\partial y} \right) + \beta T \left(\frac{\partial P}{\partial t} + V_x \frac{\partial P}{\partial x} + V_y \frac{\partial P}{\partial y} \right) + \\ P \left(\frac{\partial V_x}{\partial x} + \frac{\partial V_y}{\partial y} \right) + \tau_{xx} \frac{\partial V_x}{\partial x} + \tau_{yy} \frac{\partial V_y}{\partial y} + \tau_{xy} \left(\frac{\partial V_y}{\partial x} + \frac{\partial V_x}{\partial y} \right) + S_E \end{aligned} \tag{10}$$

For HTF and PCM having constant density and viscosity, Eq. (10) becomes:

$$\rho C_p \left(\frac{\partial T}{\partial t} + V_x \frac{\partial T}{\partial x} + V_y \frac{\partial T}{\partial y} \right) = k \left(\frac{\partial^2 T}{\partial x^2} + \frac{\partial^2 T}{\partial y^2} \right) + \beta T \left(\frac{\partial P}{\partial t} + V_x \frac{\partial P}{\partial x} + V_y \frac{\partial P}{\partial y} \right) + S_E \tag{11}$$

Where β is the thermal expansion coefficient and equal to $\frac{-1}{\rho} \left(\frac{\partial \rho}{\partial T} \right)$

$$\text{Where } S_E = \begin{cases} 0 & \text{for HTF} \\ h_f \frac{\partial Y}{\partial t} & \text{for PCM material} \end{cases}$$

For the fins that have constant density and viscosity, Eq. (10) becomes :

$$\rho C_p \frac{\partial T}{\partial t} = k \left(\frac{\partial^2 T}{\partial x^2} + \frac{\partial^2 T}{\partial y^2} \right) \tag{12}$$

The total energy change in PCM material is equal to

$$\Delta E = m \Delta h \tag{13}$$

$$\Delta E = \int \rho \Delta h \, dVol \tag{14}$$

where,

$$\Delta h = \int_{T_1}^{T_2} c_p \, dT + \Delta Y \, h_f \tag{15}$$

Boussinesq model is used to study the natural-convective flow-through liquid PCM. So, the density variation is defined as:

$$\rho = \rho_0 (1 - \beta \Delta T) \tag{16}$$

The continuity, momentum, and energy equations are numerically solved by using the ANSYS - Fluent software. Two dimensional ($\frac{\partial}{\partial z} = 0$) simulation is done by using the finite volume method [25]. ANSYS Fluent divides the domain into discrete control volumes using a computational grid. After that, Fluent integrates the governing equations on the individual control volumes to construct algebraic equations for the discrete dependent variables (velocities, pressure, temperature, and conserved scalars). Finally, Fluent makes the discretized equations and the solution of the resulting linear equation system linear to yield updated values of the dependent variables.

An enthalpy-porosity formulation [26] is used. Therefore, the solid-liquid zone is treated as a porous zone. The liquid fraction is equal to the porosity. For pressure-velocity coupling, the Pressure-Implicit with Splitting of Operators (PISO) scheme is used [27]. The PISO scheme repeats the calculation until the balance is satisfied and uses two additional corrections (neighbor and skewness corrections). The discretization is done by using the second-order upwind and PRESTO [28], [29]. The gradient of the scalars at the center of the cell is calculated by Least Squares Cell-Based Gradient method. For achieving the time-independent solution, the Courant-Friedrichs-Levy (CFL) number was set to be 1 [30] by setting the minimum mesh cell length to be 6×10^{-3} and the time step to be 0.1s.

RESULTS AND DISCUSSION

In this study, the effect of the exhaust gas temperature is studied at the design point, part, and overload, as shown in Table 2.

Table 2. Exhaust gas temperature variation

Plant Load	Exhaust gas temperature, K
100 %	400.65
75 %	393.1
50 %	392
25 %	389.5

Design Point

Combined Cycle

For preventing water vapor condensation, the exhaust gas temperature must remain higher than 100 °C. So that, the exhaust gas only has 0.033 of the burned fuel energy. Table 3 shows the state's temperature, pressure, and mass flow rate at each state of a real combined power cycle in the south of Jordan. Whereas, Table 4 shows the combined cycle performance parameter.

Table 3. Fluid states of the combined cycle

State number	Fluid type	State temperature, °C	State pressure (bar)	State flow rate (kg/h) x 10 ³
1	Air	36	0.927	1557.5 x 2
2	Air	-	-	-
3	Gas	-	-	-
4	Gas	561.3	0.961	1586.4 x 2
5	Gas	127.5	0.927	1586.4 x 2
11	Water	59.3	-	256.8
12	Water	169.4	-	241
13	Water	-	-	-
14	Water	180.3	-	210.1
15	Water	182.6	-	210.1
16	Steam	535.5	76.2	418.4
17	Steam	-	-	-
18	Steam	204.2	5.2	61.9
19	Steam	-	-	-
20	Water	57.9	0.181	479.6
21	Water	55.7	0.163	482.5

Table 4. Combined cycle performance parameters

Parameter	Value
Ambient temperature, °C	36
Fuel low heat value, kJ/kg	49,322
Fuel high heat value, kJ/kg	54,293
Fuel flow rate, kg/s	8.06 x 2
Net power generation, kW	377793

Paraffin Melting System

In the melting system, the water is heated up to 368.15 K. After that, this water is pumped to the melting container to melt the paraffin. Table 5 shows the performance parameters of this system at the design point.

Table 5. The performance parameter of the paraffin melting system

Parameter	Value	Parameter	Value
Q_{melting} , kW	1431	M_{water} , kg/s	40
$A_{\text{heatexchanger}}$, kW	1321	$\Delta P_{\text{heat exchanger}}$, Pa	223.5
$\epsilon_{\text{heatexchanger}}$	0.67	ΔP_{pump} , Pa	6591
M_{gas} , kg/s	47.35	Power Consumption, kW	14.042

A published experiment by Kamkari et al. [31] is used to validate the Ansys-Fluent software. The experiment consists of a rectangular enclosure with an inside dimension of 50 mm in width, 120 mm in height, and 120 mm in depth. The bottom wall of the enclosure (Horizontal Case, $\theta = 0$) was held at a constant temperature equal to 70 °C, whereas the other five walls of the enclosure were insulated ($k = 0.042$ W/m K). Acid with 99% purity was used as the PCM with thermophysical properties listed in Table 1, [31]. After that, we used Ansys to numerically simulate this experiment. The numerical and experimental melt mass fraction inside the enclosure are compared in Figure 4. This figure shows that the numerical results by our simulation setup are compatible with the experimental results that done by Kamkari et al.

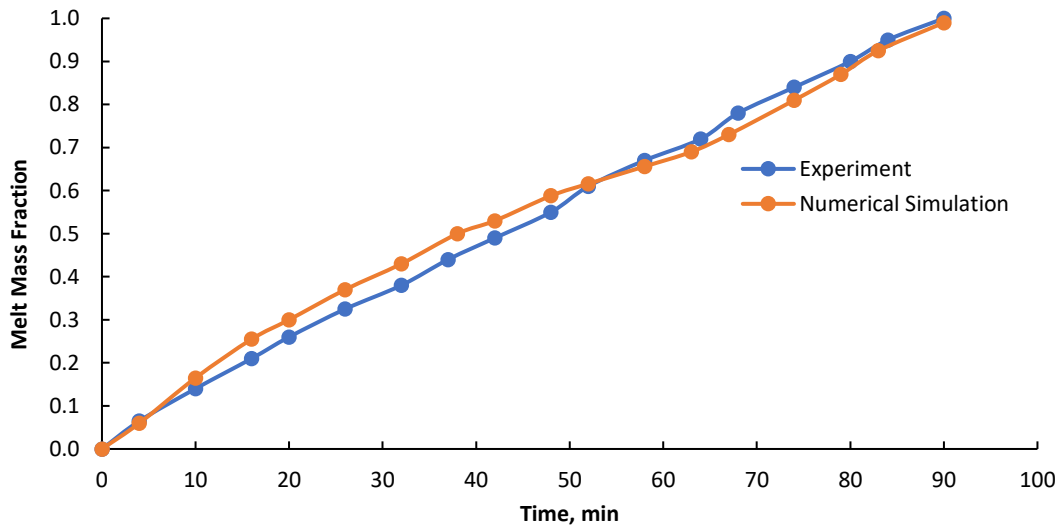


Figure 4. Experimental and numerical melt mass fraction with time

Ansys-Fluent software is also used to study the independent mesh test on four mesh models with 5244, 11659, 25773, and 54481 elements. Table 6 shows the average temperature in the paraffin, while Table 7 shows the melt mass fractions of the four models. These tables show that the model 25773 elements leads to accurate simulation results.

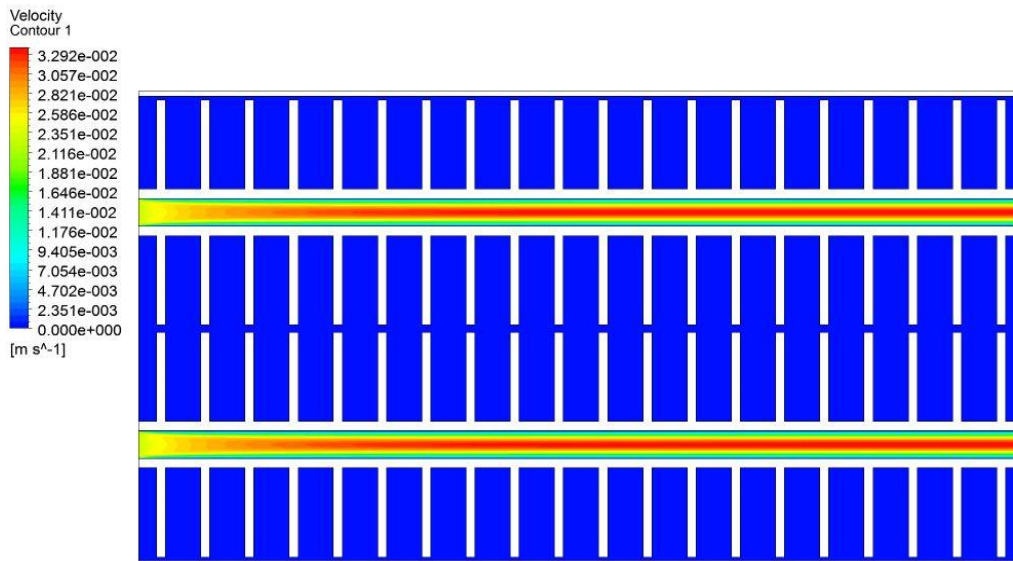
Table 6. Paraffins' average temperature results of independent mesh test

Time	Average Temperature			
	5244 elements	11659 elements	25773 elements	54481 elements
-				
900	321.056	323.452	319.609	319.619
1400	326.001	330.702	323.141	323.474
1800	331.151	338.085	326.62	327.226
2200	338.238	346.335	331.229	331.81
2700	348.247	355.243	338.571	338.238
3200	356.193	360.75	346.556	344.781
3600	360.206	363.398	352.464	349.644
3900	362.279	364.714	356.145	352.902

Table 7. Melt mass fraction results of independent mesh test

Time	Melt PCM mass fraction			
	5244 elements	11659 elements	25773 elements	54481 elements
-				
900	0.37417	0.467693	0.263352	0.266601
1400	0.645861	0.731581	0.498061	0.481664
1800	0.827071	0.885754	0.666443	0.634904
2200	0.945794	0.967715	0.805155	0.76463
2700	0.996637	0.995551	0.92441	0.886073
3200	1	1	0.983501	0.960096
3600	1	1	0.998478	0.988764
3900	1	1	1	1

Figure 5 shows the velocity distribution of the heat transfer fluid. As shown, the HTF contacting the duct is static due to the effect of no-slip condition. The cumulative of the melt mass fraction during the charging process is shown in Figures 6- 12 starting from $t = 300$ s until 3900 s with an increment of 600 s. The melt mass fraction at the starting of melting is zero, which means that the status of the paraffin is solid. HTF has a higher temperature than the Paraffin temperature. This temperature difference will lead to the transfer of the heat from the HTF to the finned tube. After that, the surfaces of the hot fins and pipes will heat the paraffin to its melting point. Therefore, the interface regions between HTF and Paraffin are firstly melted, then the melt fraction propagates. During this process before melting the whole Paraffin, the melt PCM mass fraction near the hottest surfaces is the highest. Also, the natural convection concentrates the melted paraffin in the upper halves.

**Figure 5.** The velocity distribution of HTF

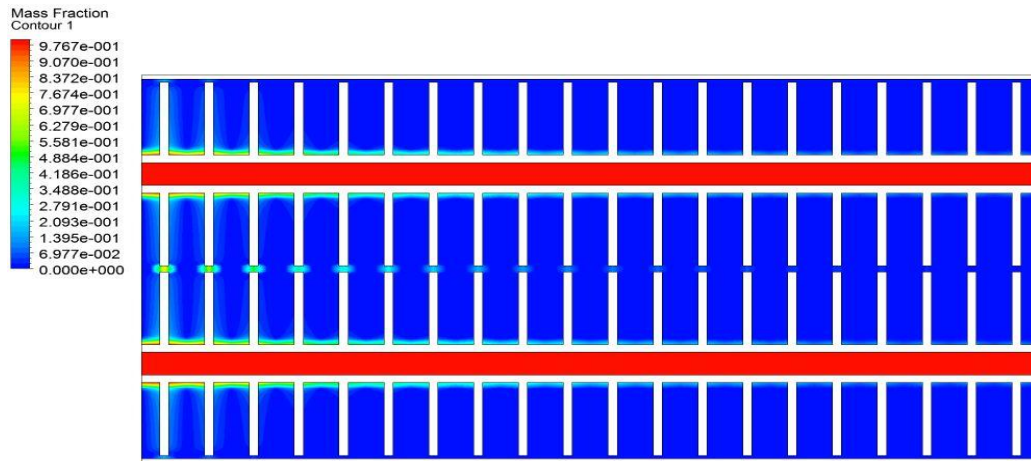


Figure 6. The melt mass fraction distribution at 300 s

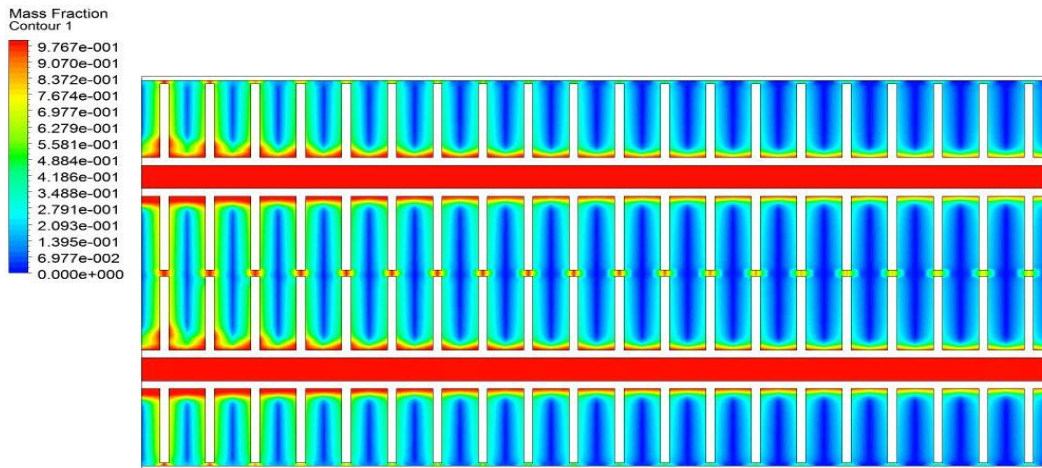


Figure 7. The melt mass fraction distribution at 900 s

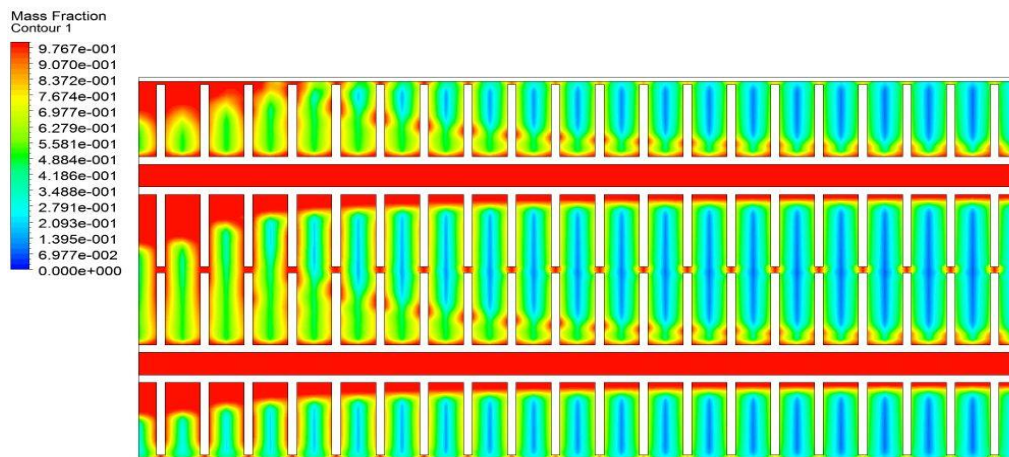


Figure 8. The melt mass fraction distribution at 1500 s

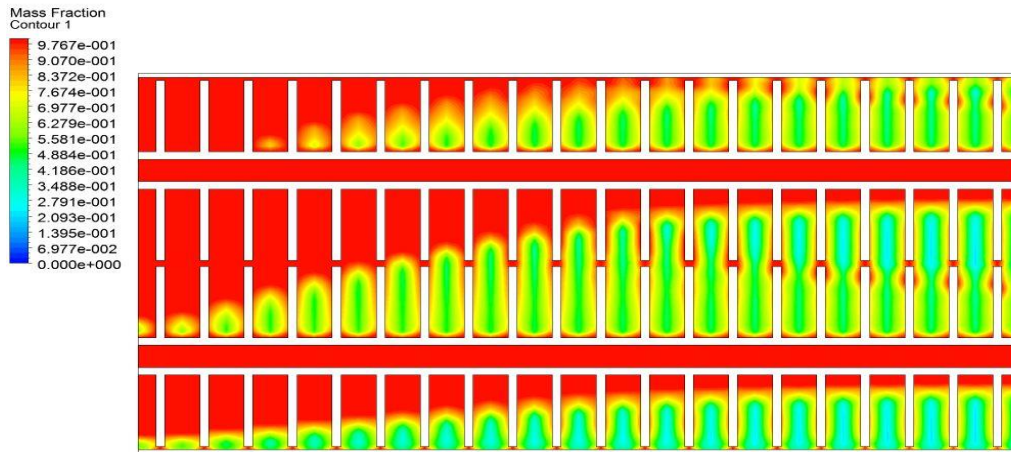


Figure 9. The melt mass fraction distribution at 2100 s

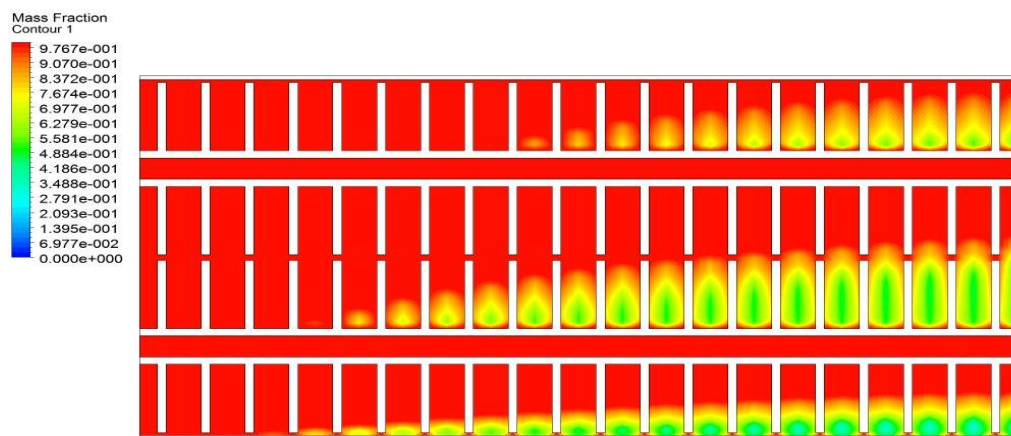


Figure 10. The melt mass fraction distribution at 2700 s

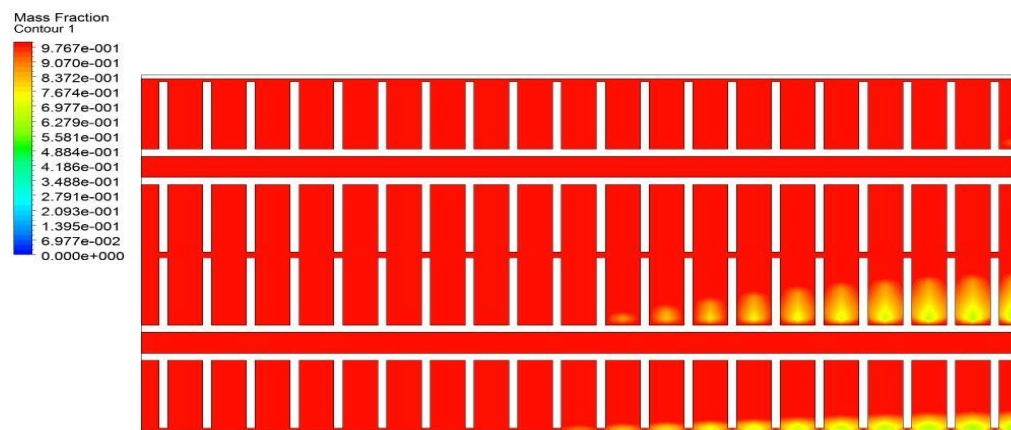


Figure 11. The melt mass fraction distribution at 3300 s

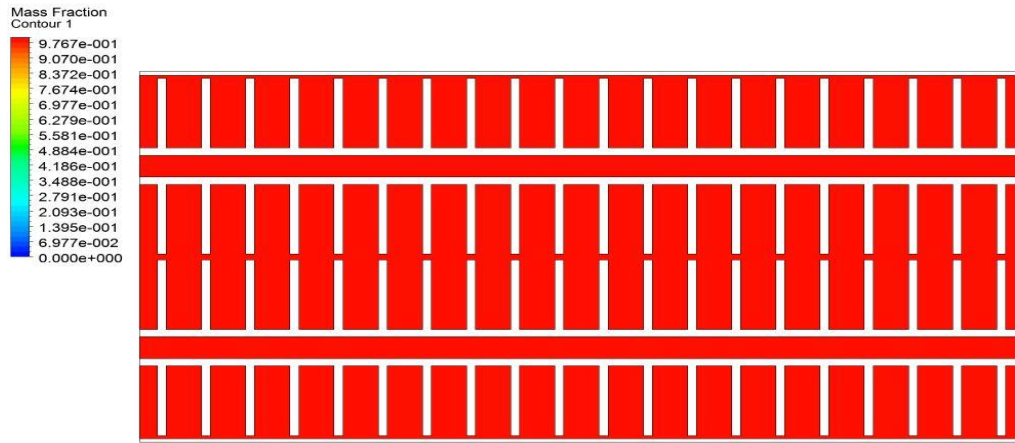


Figure 12. The melt mass fraction distribution at 3900 s

Figures 13-19 show the temperature distribution of the paraffin wax beginning from $t = 300$ s until the end of the melting process. The HTF heats the walls of the pipes, which heats the paraffin. The heat transfers by conduction through the solid paraffin and metal, whereas the natural convection is responsible for the heat transfer through the melt regions. Due to natural convection, the upper halves have the highest temperature. Also, the region near the inlet has the highest temperature.

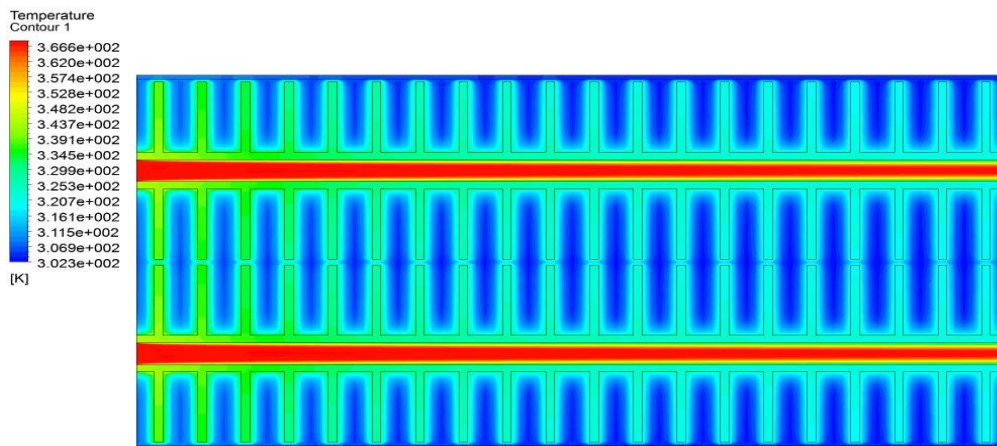


Figure 13. The temperature distribution at 300 s

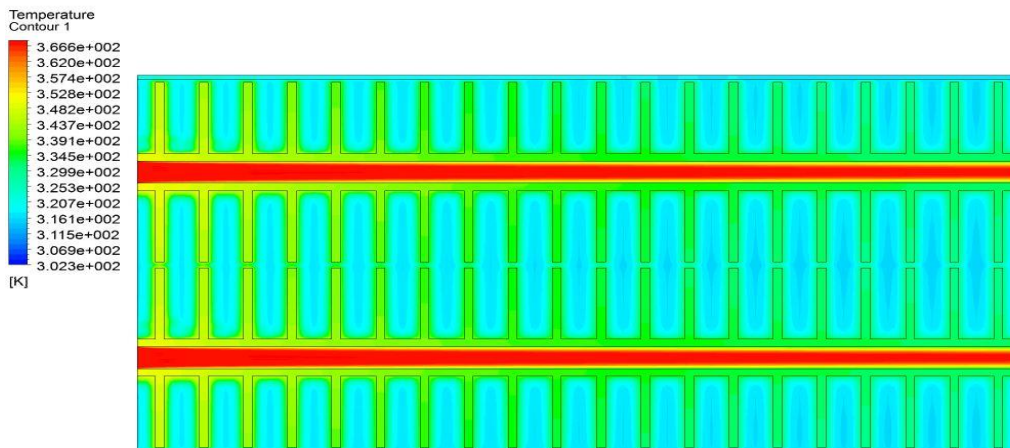


Figure 14. The temperature distribution at 900 s

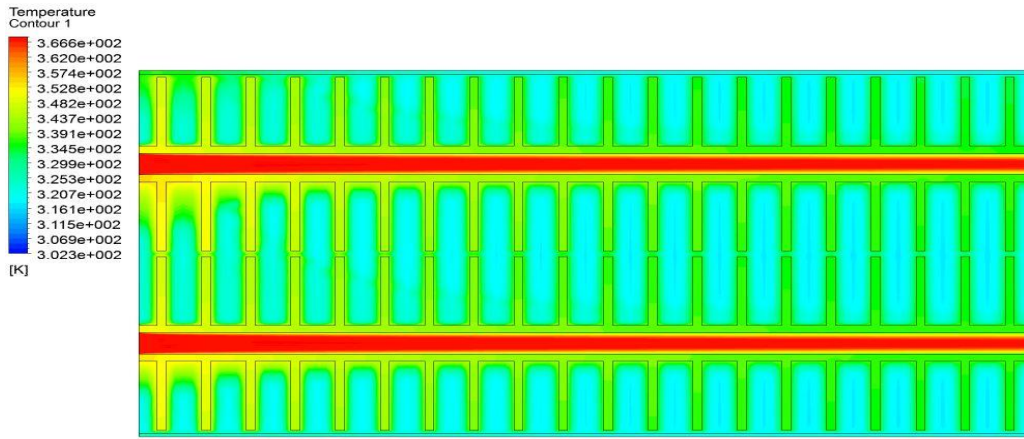


Figure 15. The temperature distribution at 1500 s

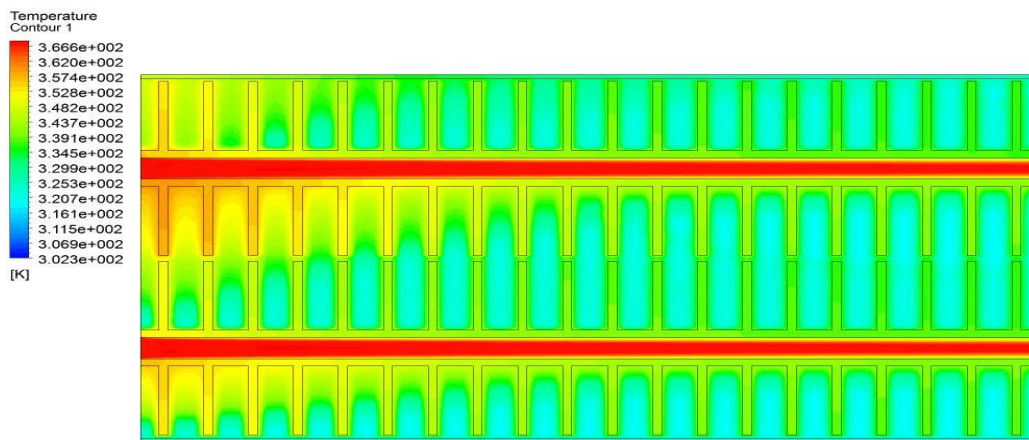


Figure 16. The temperature distribution at 2100 s

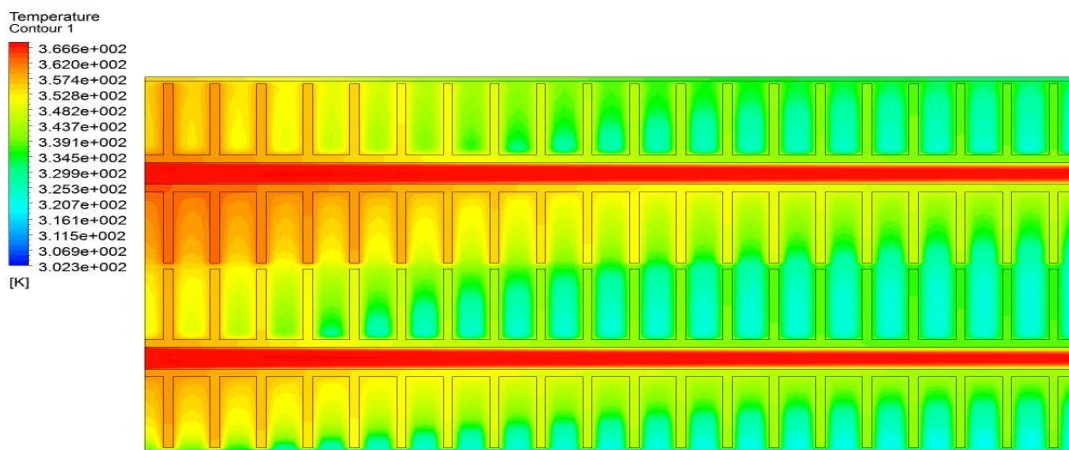


Figure 17. The temperature distribution at 2700 s

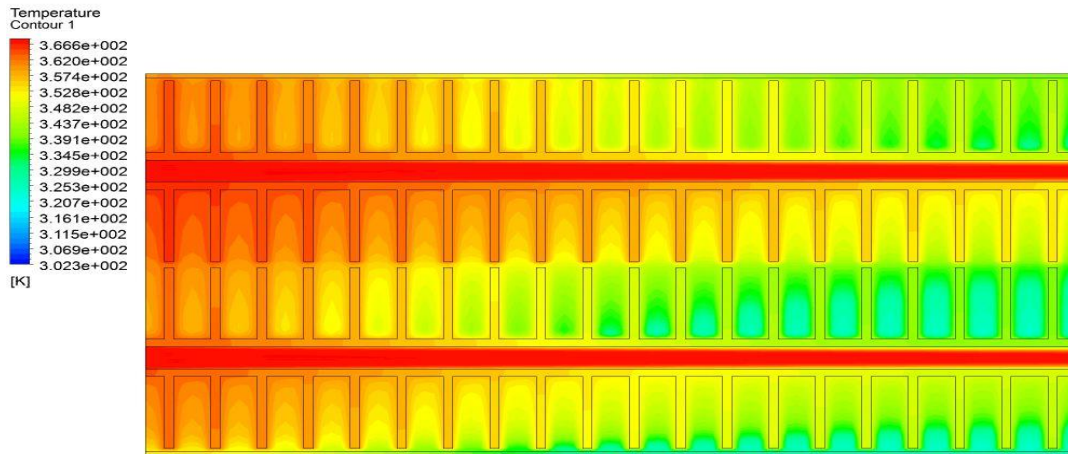


Figure 18. The temperature distribution at 3300 s

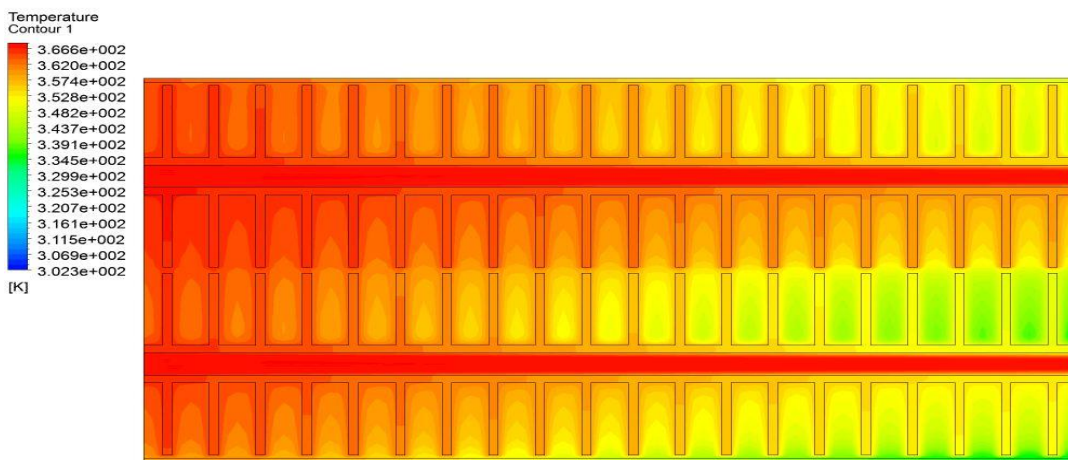


Figure 19. The temperature distribution at 3900 s

Figure 20 shows the temperature distribution at the melting container exit. The exit temperature increases with the time because the transferred heat to the paraffin wax decreases with the time. Figure 21 shows the temperature distribution at the exit of the melting system heat exchanger. As the container exit temperature increases, the heat exchanger exit temperature will increase.

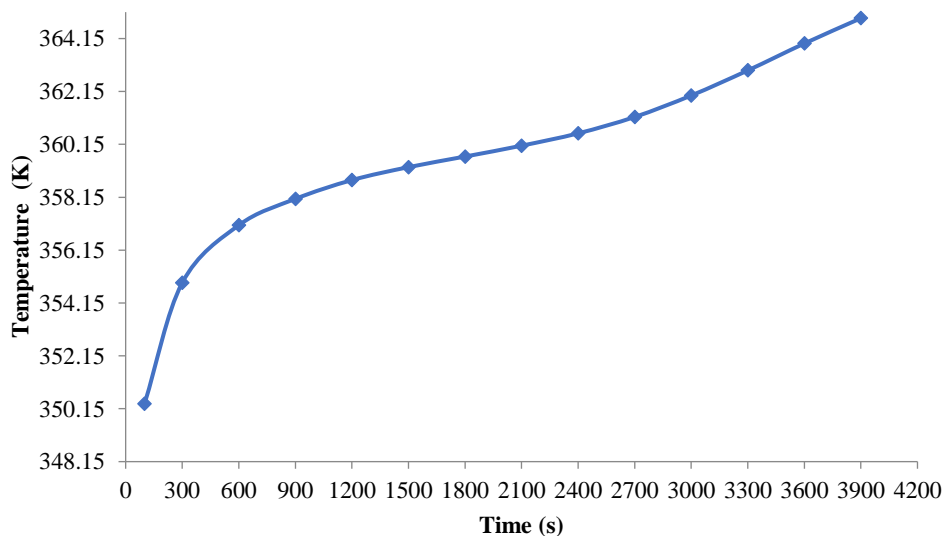


Figure 20. The temperature distribution at the container exit (point 9, Figure 1)

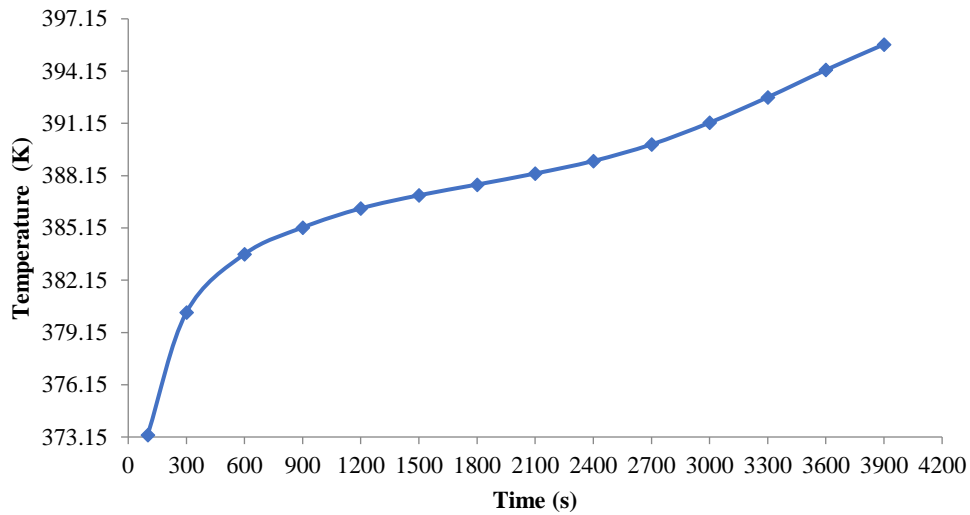


Figure 21. The temperature distribution at the exit of the melting system heat exchanger (point 8, Figure 1)

Off-Design Characteristics

Paraffin Melting System

The effect of the exhaust gas temperature (T_E) on the mass flow rate of the exhaust gas (M_E) and system power consumption (PE) are studied. In Figure 22, when exhaust gas temperature increases, the exhaust mass flow rate and cycle power consumption will decrease.

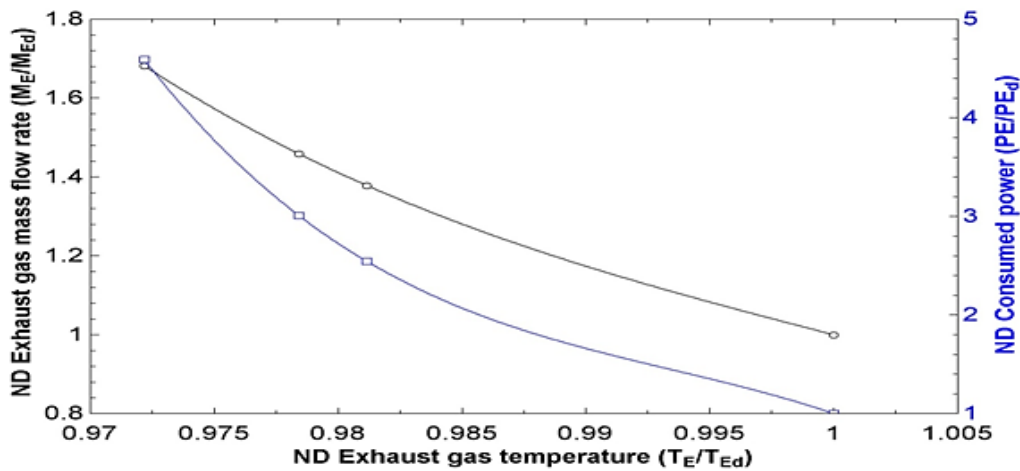


Figure 22. Effect of exhaust gas temperature on the exhaust mass flow rate and power consumption

ECONOMIC EVALUATION

The heat exchanger cost and pump cost are calculated based on [32] as :

$$C_{\text{heat exchanger}} = 7900 (A_{HE}/100)^{0.6} \tag{17}$$

$$C_{\text{pump}} = 3540 PE_p^{0.6} \tag{18}$$

Five layered paraffin wax containers are needed for a factory that produces 1100 tons per month. In an ordinary candles factory, liquefied petroleum gas (LPG) is used to melt the paraffin. LPG caloric value is 46.1 MJ/kg. This ordinary factory monthly needs 7052 kg LPG to melt this paraffin amount. This LPG costs about 5794 \$/month. The new melting system consumes 14.24 kW to melt the paraffin wax, which costs 2153 \$/month. So, the saving is 63% of the LPG cost.

Based on [33], the total capital cost of the paraffin wax container, which includes preparing the material, welding, post-weld operation, heat treatment, and inspection, is 233% of the raw material cost. The cost of raw material is 3 \$/kg, [34]. The melting system cost is the summation of the pump, compact heat exchanger and pipes cost, which is 33359 \$, and paraffin wax container cost, which is 71008 \$. Based on the melting system cost, which is 104367 \$ and the monthly saving, the payback period is 2.4 years.

CONCLUSIONS

This work covers waste energy utilization of the combined power cycle that has variable inlet guide vanes to control system results in the exhaust gas with constant temperature by using the tail energy for the paraffin wax melting process. The results are summarized below:

1. As exhaust gas temperature increases, the needed exhaust gas flow rate will decrease, which will decrease the consumption power of the system.
2. Hot surfaces firstly melt the Paraffin that contact with it and increase its temperature than other locations.
3. Natural convection causes melting the upper halves of the melting container faster than the lower halves.
4. Waste energy recovery saves 63% of the LPG cost that is ordinarily used to melt the Paraffin.
5. The payback periods of the paraffin melting system is 2.4 years.

REFERENCES

- [1] Y. S. H. Najjar and M. S. Zaamout, "Enhancing gas-turbine engine performance by means of the evaporative regenerative cycle," *Journal of the Energy Institute*, vol. 69, no. 478, pp. 1–8, 1996.
- [2] Y. Najjar, M. Akyurt, O. Al-Rabghi, and T. Alp, "Cogeneration with gas turbine engines," *Heat Recovery Systems and CHP*, vol. 13, no. 5, pp. 471–480, 1993.
- [3] Y. S. H. Najjar and M. S. Zaamout, "Comparative performance of closed cycle gas turbine engine with heat recovery using different gases," *Heat Recovery Systems and CHP*, vol. 12, no. 6, pp. 489–495, 1992, doi: 10.1016/0890-4332(92)90017-C.
- [4] Y. S. H. Najjar, "A cryogenic gas turbine engine using hydrogen for waste heat recovery and regasification of LNG," *International Journal of Hydrogen Energy*, vol. 16, no. 2, pp. 129–134, 1991, doi: 10.1016/0360-3199(91)90039-L.
- [5] Y. S. H. Najjar and A. M. Abubaker, "Indirect evaporative combined inlet air cooling with gas turbines for green power technology," *International Journal of Refrigeration*, vol. 59, no. February 2018, pp. 235–250, 2015, doi: 10.1016/j.ijrefrig.2015.07.001.
- [6] Y. S. H. Najjar and A. M. Abubaker, "Thermoeconomic analysis and optimization of a novel inlet air cooling system with gas turbine engines using cascaded waste-heat recovery," *Energy*, vol. 128, no. January, pp. 421–434, 2017, doi: 10.1016/j.energy.2017.04.029.
- [7] O. K. Singh, "Performance enhancement of combined cycle power plant using inlet air cooling by exhaust heat operated ammonia-water absorption refrigeration system," *Applied Energy*, vol. 180, pp. 867–879, 2016, doi: 10.1016/j.apenergy.2016.08.042.
- [8] C. Carcasci and L. Winchler, "Thermodynamic Analysis of an Organic Rankine Cycle for Waste Heat Recovery from an Aero-derivative Intercooled Gas Turbine," *Energy Procedia*, vol. 101, no. September, pp. 862–869, 2016, doi: 10.1016/j.egypro.2016.11.109.
- [9] D. T. Bălănescu and V. M. Homutescu, "Performance analysis of a gas turbine combined cycle power plant with waste heat recovery in Organic Rankine Cycle," *Procedia Manufacturing*, vol. 32, pp. 520–528, 2019, doi: 10.1016/j.promfg.2019.02.248.
- [10] O. Ipakchi, A. H. Mosaffa, and L. Garousi Farshi, "Ejector based CO₂ transcritical combined cooling and power system utilizing waste heat recovery: A thermoeconomic assessment," *Energy Conversion and Management*, vol. 186, no. March, pp. 462–472, 2019, doi: 10.1016/j.enconman.2019.03.009.
- [11] B. C. Han, W. L. Cheng, Y. Y. Li, and Y. Le Nian, "Thermodynamic analysis of heat driven Combined Cooling Heating and Power system (CCHP) with energy storage for long distance transmission," *Energy Conversion and Management*, vol. 154, no. October, pp. 102–117, 2017, doi: 10.1016/j.enconman.2017.10.058.
- [12] Z. Huang, C. Yang, H. Yang, and X. Ma, "Ability of adjusting heating/power for combined cooling heating and power system using alternative gas turbine operation strategies in combined cycle units," *Energy Conversion and Management*, vol. 173, no. 8, pp. 271–282, 2018, doi: 10.1016/j.enconman.2018.07.062.
- [13] S. Hou *et al.*, "Optimization of a combined cooling, heating and power system using CO₂ as main working fluid driven by gas turbine waste heat," *Energy Conversion and Management*, vol. 178, no. September, pp. 235–249, 2018, doi: 10.1016/j.enconman.2018.09.072.
- [14] B. Dehghan B., "Performance assessment of ground source heat pump system integrated with micro gas turbine: Waste heat recovery," *Energy Conversion and Management*, vol. 152, no. September, pp. 328–341, 2017, doi: 10.1016/j.enconman.2017.09.058.

- [15] C. Yang, X. Wang, M. Huang, S. Ding, and X. Ma, "Design and simulation of gas turbine-based CCHP combined with solar and compressed air energy storage in a hotel building," *Energy Build.*, vol. 153, pp. 412–420, 2017, doi: 10.1016/j.enbuild.2017.08.035.
- [16] X. Wang, C. Yang, M. Huang, and X. Ma, "Off-design performances of gas turbine-based CCHP combined with solar and compressed air energy storage with organic Rankine cycle," *Energy Conversion and Management.*, vol. 156, no. 30, pp. 626–638, 2018, doi: 10.1016/j.enconman.2017.11.082.
- [17] B. Grange, C. Dalet, Q. Falcoz, A. Ferrière, and G. Flamant, "Impact of thermal energy storage integration on the performance of a hybrid solar gas-turbine power plant," *Applied Thermal Engineering*, vol. 105, pp. 266–275, 2016, doi: 10.1016/j.applthermaleng.2016.05.175.
- [18] M. Abar, B. Geels, J. Hertzberg, and L. D. Montoya, "Pumped thermal energy storage and bottoming system part A: Concept and model," *Energy*, vol. 120, pp. 320–331, 2017, doi: 10.1016/j.energy.2016.11.089.
- [19] P. T. Weber, "Modeling Gas Turbine Engine Performance at Part-Load," University of Wyoming, 2011.
- [20] A. S. Irbai and Y. S. H. Najjar, "Enhancement of the melting process in the thermal energy storage system by using novel geometry," *Numerical Heat Transfer, Part A: Applications*, vol. 76, no. 12, pp. 1006–1022, 2019, doi: 10.1080/10407782.2019.1673109.
- [21] Z. Li and Z. G. Wu, "Analysis of HTFs, PCMs and fins effects on the thermal performance of shell-tube thermal energy storage units," *Solar Energy*, vol. 122, pp. 382–395, 2015, doi: 10.1016/j.solener.2015.09.019.
- [22] A. Dinker, M. Agarwal, and G. D. Agarwal, "Heat storage materials, geometry and applications: A review," *Journal of the Energy Institute*, vol. 90, no. 1, pp. 1–11, 2017, doi: 10.1016/j.joei.2015.10.002.
- [23] F. P. Incropera, D. P. DeWitt, T. L. Bergman, and A. S. Lavine, *Fundamentals of heat and mass transfer*, Sixth. Hoboken: John Wiley & Sons, 2007.
- [24] L. C. Burmeister, *Convective heat transfer*, Second. New York: John Wiley & Sons, 1993.
- [25] S. Patankar, *Numerical heat transfer and fluid flow*. New York: Hemisphere, 1980.
- [26] V. R. Voller and C. Prakash, "A fixed grid numerical modelling methodology for convection-diffusion mushy region phase-change problems," *International Journal of Heat and Mass Transfer*, vol. 30, no. 8, pp. 1709–1719, 1987, doi: 10.1016/0017-9310(87)90317-6.
- [27] H. Versteeg and W. Malalasekera, *An introduction to Computational Fluid Dynamics*. Harlow: Longman, 1995.
- [28] Ansys, "Ansys Help Tutorial." Ansys.
- [29] T. J. Barth and D. C. Jespersen, "The design and application of upwind schemes on unstructured meshes," in *27th Aerospace Sciences Meeting*, 1989, p. 13.
- [30] Z. I. Al-Hashimy, H. H. Al-Kayiem, R. W. Time, and Z. K. Kadhim, "Numerical characterisation of slug flow in horizontal air/water pipe flow," *International Journal of Computational Methods and Experimental Measurements*, vol. 4, no. 2, pp. 114–130, 2016, doi: 10.2495/CMEM-V4-N2-114-130.
- [31] B. Kamkari, H. Shokouhmand, and F. Bruno, "Experimental investigation of the effect of inclination angle on convection-driven melting of phase change material in a rectangular enclosure," *International Journal of Heat and Mass Transfer*, vol. 72, pp. 186–200, 2014, doi: 10.1016/j.ijheatmasstransfer.2014.01.014.
- [32] A. Behzadi, E. Gholamian, E. Houshfar, and A. Habibollahzade, "Multi-objective optimization and exergoeconomic analysis of waste heat recovery from Tehran's waste-to-energy plant integrated with an ORC unit," *Energy*, vol. 160, no. July, pp. 1055–1068, 2018, doi: 10.1016/j.energy.2018.07.074.
- [33] G. Shrijit, "How to Become Successful in Welding Business," *Your Article Library*. <http://www.yourarticlelibrary.com/welding/how-to-become-successful-in-welding-business/98008>.
- [34] Alibaba Company, "Copper," 2018. <https://www.alibaba.com/>.